THE EUROPEAN
PHYSICAL JOURNAL C

Observation of $\Xi_b^0 \to \Xi_c^+ D_s^-$ and $\Xi_b^- \to \Xi_c^0 D_s^-$ decays

LHCb collaboration[*]

CERN, 1211 Geneva 23, Switzerland

Abstract The $\Xi_b^0 \to \Xi_c^+ D_s^-$ and $\Xi_b^- \to \Xi_c^0 D_s^-$ decays are observed for the first time using proton-proton collision data collected by the LHCb experiment at a centre-of-mass energy of $\sqrt{s} = 13$ TeV, corresponding to an integrated luminosity of 5.1 fb^{-1}. The branching fractions times the production cross-sections of Ξ_b baryons relative to that of Λ_b^0 baryon are measured to be

$$\mathcal{R}\left(\frac{\Xi_b^0}{\Lambda_b^0}\right) \equiv \frac{\sigma\left(\Xi_b^0\right)}{\sigma\left(\Lambda_b^0\right)} \times \frac{\mathcal{B}\left(\Xi_b^0 \to \Xi_c^+ D_s^-\right)}{\mathcal{B}\left(\Lambda_b^0 \to \Lambda_c^0 D_s^-\right)}$$
$$= (15.8 \pm 1.1 \pm 0.6 \pm 7.7)\%,$$

$$\mathcal{R}\left(\frac{\Xi_b^-}{\Lambda_b^0}\right) \equiv \frac{\sigma\left(\Xi_b^-\right)}{\sigma\left(\Lambda_b^0\right)} \times \frac{\mathcal{B}\left(\Xi_b^- \to \Xi_c^0 D_s^-\right)}{\mathcal{B}\left(\Lambda_b^0 \to \Lambda_c^0 D_s^-\right)}$$
$$= (16.9 \pm 1.3 \pm 0.9 \pm 4.3)\%,$$

where the first uncertainties are statistical, the second systematic, and the third due to the uncertainties on the decay branching fractions of relevant charmed baryons. The masses of Ξ_b^0 and Ξ_b^- baryons are measured to be $m_{\Xi_b^0} = 5791.12 \pm 0.60 \pm 0.45 \pm 0.24$ MeV/c^2 and $m_{\Xi_b^-} = 5797.02 \pm 0.63 \pm 0.49 \pm 0.29$ MeV/c^2, where the uncertainties are statistical, systematic, and those due to charmed-hadron masses, respectively.

1 Introduction

Hadrons are systems of quarks bound by the strong interaction, described at the fundamental level by quantum chromodynamics (QCD). The production and decay of hadrons involve the nonperturbative regime of QCD, making calculations challenging. Much progress has been made in recent years in experimental and theoretical studies of beauty mesons, with the aim of testing the Standard Model and

A. Gomes: Deceased

[*] e-mail: yshang@cern.ch

searching for new physics through measurements of branching fractions, CP asymmetries and rare decays [1]. However, many aspects of beauty baryons are still largely unknown, due to the difficulties to produce and detect them in experiments other than those operating at the Large Hadron Collider.

So far, the Λ_b^0 baryon has been more widely studied than the other beauty baryons, including Ξ_b^0 and Ξ_b^-.[1] Very few decay modes have been measured for $\Xi_b^{0(-)}$ baryons [2]. According to the quark model, the three beauty baryons Λ_b^0, Ξ_b^0 and Ξ_b^- (referred to as H_b in the following) form an $SU(3)$ flavour multiplet, as do the Λ_c^+, Ξ_c^+ and Ξ_c^0 states (referred to as H_c in the following). The H_b decay is dominated by the weak transition of the b quark while the two light quarks serve as compact spectators [3,4]. According to heavy quark effective theory, the three decays of bottom baryons into two charmed hadrons, $H_b \to H_c D_s^-$, should have approximately the same partial width [5,6]. The $\Lambda_b^0 \to \Lambda_c^+ D_s^-$ decay has been measured to have a branching fraction ($\mathcal{B}$) at the percent level [7], but no measurements for $\Xi_b^{0(-)} \to \Xi_c^{+(0)} D_s^-$ decays are available. Measurements of these decays not only test the $SU(3)$ symmetry but also give insights into the dynamics of weak decays of beauty baryons.

Beauty baryons of all species are abundantly produced at the LHC [8–11], allowing them to be intensively studied. This analysis presents the first observation of $\Xi_b^0 \to \Xi_c^+ D_s^-$ and $\Xi_b^- \to \Xi_c^0 D_s^-$ decays, using data from proton-proton (pp) collisions at a centre-of-mass energy of $\sqrt{s} = 13$ TeV collected by LHCb detector and corresponding to an integrated luminosity of 5.1 fb^{-1}. The relative production rates of the decays, $\mathcal{R}$, defined to be

$$\mathcal{R}\left(\frac{\Xi_b^0}{\Lambda_b^0}\right) \equiv \frac{\sigma\left(\Xi_b^0\right)}{\sigma\left(\Lambda_b^0\right)} \times \frac{\mathcal{B}\left(\Xi_b^0 \to \Xi_c^+ D_s^-\right)}{\mathcal{B}\left(\Lambda_b^0 \to \Lambda_c^+ D_s^-\right)}, \tag{1}$$

$$\mathcal{R}\left(\frac{\Xi_b^-}{\Lambda_b^0}\right) \equiv \frac{\sigma\left(\Xi_b^-\right)}{\sigma\left(\Lambda_b^0\right)} \times \frac{\mathcal{B}\left(\Xi_b^- \to \Xi_c^0 D_s^-\right)}{\mathcal{B}\left(\Lambda_b^0 \to \Lambda_c^+ D_s^-\right)}, \tag{2}$$

---

[1] The inclusion of charge-conjugate processes is implied throughout.

$$\mathcal{R}\left(\frac{\varXi_b^0}{\varXi_b^-}\right) \equiv \frac{\sigma\left(\varXi_b^0\right)}{\sigma\left(\varXi_b^-\right)} \times \frac{\mathcal{B}\left(\varXi_b^0 \to \varXi_c^+ D_s^-\right)}{\mathcal{B}\left(\varXi_b^- \to \varXi_c^0 D_s^-\right)}, \tag{3}$$

are measured, where σ denotes the production cross-section. Given the similar lifetimes of the three beauty baryons [2], if the decay widths of the three beauty-baryon decays are also similar, the variables defined in Eqs. (1)–(3) provide measurements of the H_b production cross-section ratios, *i.e. b*-quark fragmentation fraction ratios. Isospin symmetry assures that $\sigma\left(\varXi_b^0\right)/\sigma\left(\varXi_b^-\right) \approx 1$ to a good approximation, resulting in $\mathcal{R}\left(\frac{\varXi_b^0}{\varXi_b^-}\right) \approx 1$ at leading order, which is tested in this analysis. The masses of the $\varXi_b^0$ and $\varXi_b^-$ baryons and the mass differences between the three beauty baryons are also measured.

2 Detector, samples and analysis strategy

The LHCb detector [12,13] is a single-arm forward spectrometer covering the pseudorapidity range $2 < \eta < 5$, designed for the study of particles containing *b* or *c* quarks. The detector includes a high-precision tracking system consisting of a silicon-strip vertex detector surrounding the *pp* interaction region, a large-area silicon-strip detector located upstream of a dipole magnet with a bending power of about 4 Tm, and three stations of silicon-strip detectors and straw drift tubes placed downstream of the magnet. The tracking system provides a measurement of the momentum, *p*, of charged particles with a relative uncertainty that varies from 0.5% at low momentum to 1.0% at 200 GeV/*c*. The momentum scale is calibrated using samples of $J/\psi \to \mu^+\mu^-$ and $B^+ \to J/\psi K^+$ decays collected concurrently with the data samples used for this analysis [14,15]. The relative uncertainty of this procedure is determined to be 3×10^{-4} using samples of other fully reconstructed *B*, Υ, and K_S^0-meson decays. The minimum distance of a track to a primary *pp* collision vertex (PV), the impact parameter (IP), is measured with a resolution of $(15+29/p_T)\,\mu\text{m}$, where p_T is the component of the momentum transverse to the beam, in GeV/*c*. Different types of charged hadrons are distinguished using information from two ring-imaging Cherenkov detectors. Photons, electrons and hadrons are identified by a calorimeter system consisting of scintillating-pad and preshower detectors, an electromagnetic and a hadronic calorimeter.

The data used in this analysis come from *pp* collisions at $\sqrt{s} = 13$ TeV, collected by LHCb between 2016 and 2018. The total integrated luminosity is 5.1 fb^{-1}. The online event selection of LHCb is performed by a trigger [16], which consists of a hardware stage, based on information from the calorimeter and muon systems, followed by a software stage, which applies a full event reconstruction. At the hard-

ware trigger stage, events are required to have a muon with high p_T or a hadron, photon or electron with high transverse energy in the calorimeters. A global hardware trigger decision is required based on the reconstructed candidate, the rest of the event, or a combination of both. The software trigger requires a two-, three- or four-track secondary vertex with a significant displacement from any primary *pp* interaction vertex. At least one charged particle within the secondary vertex must have a transverse momentum $p_T > 1.6$ GeV/*c* and be inconsistent with originating from any PV.

Simulated decays are used to perform event selections, calculate reconstruction and selection efficiencies, and determine the invariant-mass distributions of the reconstructed signal H_b candidates. In the simulation, *pp* collisions are generated using PYTHIA 8 [17] with a specific LHCb configuration [13]. Decays of unstable particles are described by EVTGEN [18], in which final-state radiation is generated using PHOTOS [19]. The interaction of the generated particles with the detector, and its response, are simulated using the GEANT4 [20] toolkit as described in Ref. [21].

The Λ_c^+ and $\varXi_c^+$ baryons are reconstructed in the $pK^-\pi^+$ final state, and the $\varXi_c^0$ baryon in the $pK^-K^-\pi^+$ final state. The D_s^- mesons are reconstructed by combining three charged particles identified as K^-, K^+ and π^- mesons. The H_c candidates are combined with D_s^- candidates to form the H_b candidates. The three $\mathcal{R}$ parameters are defined as

$$\mathcal{R}\left(\frac{\varXi_b^0}{\Lambda_b^0}\right) = \frac{N\left(\varXi_b^0 \to \varXi_c^+ D_s^-\right)/\varepsilon\left(\varXi_b^0 \to \varXi_c^+ D_s^-\right)}{N\left(\Lambda_b^0 \to \Lambda_c^+ D_s^-\right)/\varepsilon\left(\Lambda_b^0 \to \Lambda_c^+ D_s^-\right)}$$
$$\times \frac{\mathcal{B}\left(\Lambda_c^+ \to pK^-\pi^+\right)}{\mathcal{B}\left(\varXi_c^+ \to pK^-\pi^+\right)}, \tag{4}$$

$$\mathcal{R}\left(\frac{\varXi_b^-}{\Lambda_b^0}\right) = \frac{N\left(\varXi_b^- \to \varXi_c^0 D_s^-\right)/\varepsilon\left(\varXi_b^- \to \varXi_c^0 D_s^-\right)}{N\left(\Lambda_b^0 \to \Lambda_c^+ D_s^-\right)/\varepsilon\left(\Lambda_b^0 \to \Lambda_c^+ D_s^-\right)}$$
$$\times \frac{\mathcal{B}\left(\Lambda_c^+ \to pK^-\pi^+\right)}{\mathcal{B}\left(\varXi_c^0 \to pK^-K^-\pi^+\right)}, \tag{5}$$

$$\mathcal{R}\left(\frac{\varXi_b^0}{\varXi_b^-}\right) = \frac{N\left(\varXi_b^0 \to \varXi_c^+ D_s^-\right)/\varepsilon\left(\varXi_b^0 \to \varXi_c^+ D_s^-\right)}{N\left(\varXi_b^- \to \varXi_c^0 D_s^-\right)/\varepsilon\left(\varXi_b^- \to \varXi_c^0 D_s^-\right)}$$
$$\times \frac{\mathcal{B}\left(\varXi_c^0 \to pK^-K^-\pi^+\right)}{\mathcal{B}\left(\varXi_c^+ \to pK^-\pi^+\right)}, \tag{6}$$

where N, ε, and $\mathcal{B}$ denote the observed signal yields, the total experimental efficiencies, and the branching fractions, respectively. The world averages of branching fractions of corresponding H_c decays [2] are summarised in Table 1. The signal yields are determined using unbinned extended maximum-likelihood fits of the $H_c D_s^-$ invariant-mass distributions. The efficiencies are determined using simulated signal decays, calibrated by data driven methods.

Table 1 Branching fractions of H_c decays [2]

| Decay	Branching fraction
$\Lambda_c^+ \to pK^-\pi^+$	$(6.28 \pm 0.32) \times 10^{-2}$
$\Xi_c^+ \to pK^-\pi^+$	$(6.2 \pm 3.0) \times 10^{-3}$
$\Xi_c^0 \to pK^-K^-\pi^+$	$(4.8 \pm 1.2) \times 10^{-3}$

3 Event selections and efficiencies

In order to suppress background due to random combinations of either the H_c or D_s^-, and misidentification of final-state particles, a series of event selections are performed. Firstly, all final-state particles are required to be separated from any PV and have $p_T > 100\,\mathrm{MeV}/c$. They must also be correctly identified, with a high significance, as either a proton, kaon or pion, using combined information from the tracking system and sub-detectors related to particle identification (PID) [12,22]. The final states of the H_c and D_s^- candidates must have a scalar sum of $p_T > 1.8\,\mathrm{GeV}/c$, and at least one of them must have $p_T > 0.5\,\mathrm{GeV}/c$ and $p > 5\,\mathrm{GeV}/c$. They are additionally required to form a good vertex that is significantly separated from any PV. The H_c and D_s^- candidates should have an invariant mass within $\pm 25\,\mathrm{MeV}/c^2$ of the previous world average mass value [2], and their vertices should be consistent with being downstream of the H_b vertex. The H_b candidate formed by the H_c and D_s^- hadrons must have a good vertex separated from its associated PV, and its momentum must point back to the associated PV. The final-state particles of the H_b must have a scalar sum of $p_T > 5\,\mathrm{GeV}/c$. Finally, H_b candidates with transverse momentum $p_T > 4\,\mathrm{GeV}/c$ and rapidity $2.5 < y < 4$ are retained for further analysis.

There are backgrounds due to genuine particle decays, where a pion or kaon decay product is misidentified as a proton, resulting in a H_c candidate. For Λ_c^+ and Ξ_c^+ candidates, they include $\phi \to K^+K^-$, $D_s^+ \to K^+K^-\pi^+$, $D^+ \to K^+K^-\pi^+$ and $D^0 \to K^+K^-$ decays with the K^+ meson misidentified as a proton, and $D^+ \to K^-\pi^+\pi^+$, $D^0 \to K^-\pi^+$ decays with the π^+ meson misidentified as a proton. For Ξ_c^0 candidates, there are backgrounds due to $\phi \to K^+K^-$ and $D^0 \to K^+K^-\pi^+$ decays with the K^+ meson misidentified as a proton. For D_s^- candidates, the $\Lambda_c^+ \to pK^-\pi^+$ background with the proton misidentified as a K^+ meson is considered. To remove these background, candidates are required to satisfy strict PID requirements or their invariant masses, calculated with alternative mass hypotheses for final states, must be outside a region around the known mass of the corresponding genuine particle (ϕ, D_s^+, D^+, D^0, or Λ_c^+) [2]. Backgrounds due to $D^- \to K^+\pi^-\pi^-$ decays are also considered, and are found to be negligible.

Further event selections are performed using a gradient-boosted decision tree (BDTG) [23] algorithm to reduce combinatorial backgrounds. Due to the similarity between the topologies of the three $H_b \to H_c D_s^-$ decays, and to benefit from a cancellation of systematic uncertainties related to the BDTG selection in the $\mathcal{R}$ measurements, the BDTG classifier is trained with the Ξ_b^0 samples and is applied to all the three decay modes. The BDTG algorithm is trained to distinguish simulated $\Xi_b^0 \to \Xi_c^+ D_s^-$ decays from the candidates in the high mass sideband ($m(\Xi_b^0) > 5950\,\mathrm{MeV}/c^2$) of data, which are representative of the background. The BDTG classifier combines seventeen variables, including kinematic, topological and PID information, to get a single discriminating response. The optimal requirement on the BDTG response is determined by maximising the figure of merit $F \equiv S/\sqrt{S + B}$, where S (B) is the expected number of signal (background) yield in the signal region of data with BDTG response greater than a given value. The signal region is defined to be $\pm 30\,\mathrm{MeV}/c^2$ around the previous world average of H_b mass [2], which is about three times the experimental resolution. The value of S is calculated as the product of the BDTG efficiency for the signal and the signal yield before the BDTG requirement, which is obtained by fitting to Ξ_b^0 invariant-mass distribution in data. Similarly, B is calculated as the background retention rate multiplied by the estimated background in the signal region without the BDTG requirement. The background retention rate is evaluated with the high-mass sideband data ($m(\Lambda_b^0) > 5700\,\mathrm{MeV}/c^2$, $m(\Xi_b^0) > 5900\,\mathrm{MeV}/c^2$, $m(\Xi_b^-) > 5900\,\mathrm{MeV}/c^2$), and the number of background candidates in the signal region is estimated with a fit to Ξ_b^0 invariant-mass distribution in the high invariant-mass sideband region of the data, with a subsequent extrapolation to the signal mass region. The optimal BDTG requirement corresponds to a signal efficiency of about 95% with respect to other selection requirements for all three H_b decay modes.

The total efficiency is calculated as the product of efficiencies of detector acceptance, reconstruction, and selection. It is estimated using the simulated signal decays. These samples are calibrated such that the shapes of several key distributions match those of the data: the PID response, H_b kinematics, total charged-track multiplicity and H_c resonant structures. The $D_s^- \to K^+K^-\pi^-$ decay is simulated using measured Dalitz compositions [24], thus no corrections are applied. The PID efficiencies for the different particle species are measured using charmed hadron samples in data [22]. The large sample of $\Lambda_b^0 \to \Lambda_c^+ D_s^-$ decays is used to correct for the transverse momentum, pseudorapidity, and charged-track multiplicity distributions of the three H_b decay modes. Further corrections are made to align the shapes of the charged-track multiplicity distributions in the data and simulation for Ξ_b decays. The H_c Dalitz distribution is compared between the data and simulation; a weight-based correction is applied
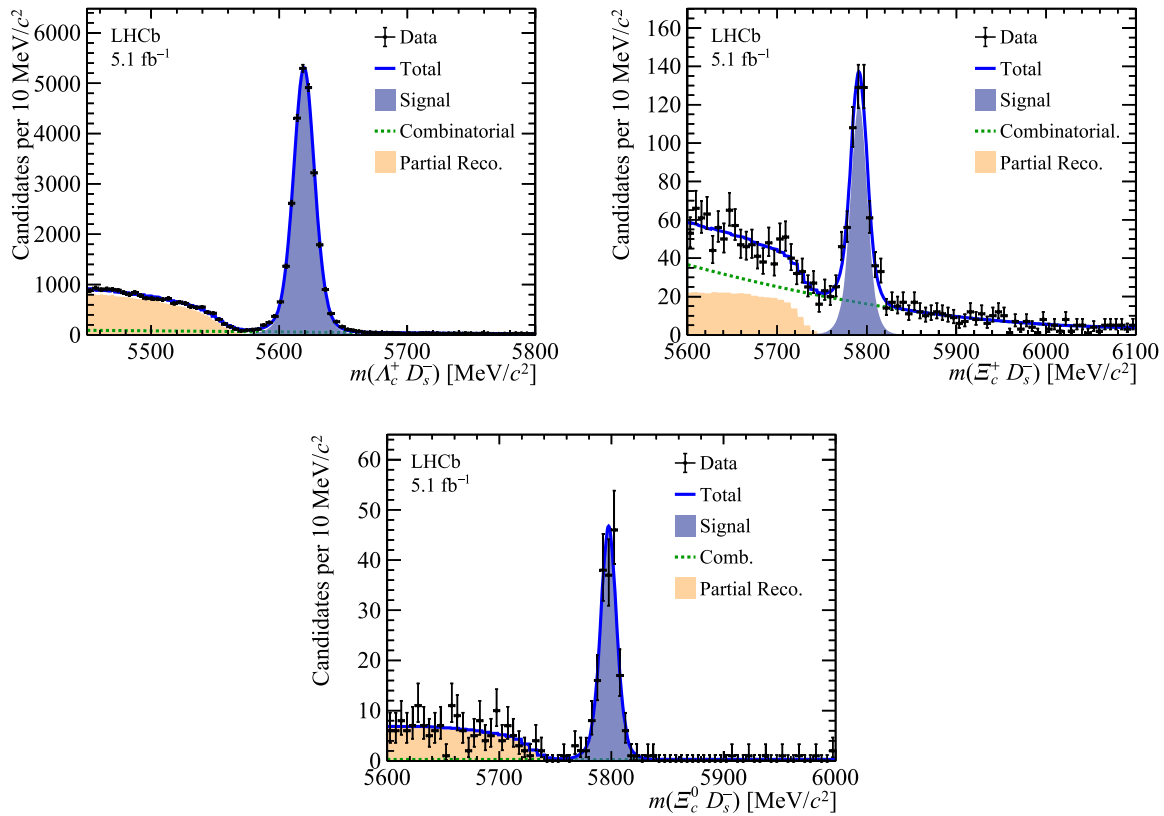
Fig. 1 Invariant-mass distributions of (top left) Λ_b^0, (top right) Ξ_b^0, and (bottom) Ξ_b^- decays. The data are overlaid on the fit results

to improve the agreement. The track-finding efficiency in simulation is found to be slightly different from that in data, and this difference is corrected as a function of the momentum and pseudorapidity of final-state particles [25]. The correction factors are generally obtained in bins of relevant variables apart from that for the Ξ_c^0 Dalitz distribution, where the large number of dimensions implies a limited number of candidates per bin. An unbinned multivariate algorithm is therefore used [26]. The ratios of efficiencies between Λ_b^0, Ξ_b^0, and Ξ_b^- decays are determined to be

$$\frac{\varepsilon(\Xi_b^0)}{\varepsilon(\Lambda_b^0)} = 1.101 \pm 0.010,$$

$$\frac{\varepsilon(\Xi_b^-)}{\varepsilon(\Lambda_b^0)} = 0.515 \pm 0.005,$$

$$\frac{\varepsilon(\Xi_b^0)}{\varepsilon(\Xi_b^-)} = 2.138 \pm 0.017,$$

where the uncertainties are statistical only. The Λ_b^0 and Ξ_b^0 decays have a similar efficiency, while the smaller Ξ_b^- efficiency is due to one more final-state particle.

4 Signal yield determination and mass measurements

To obtain the yields of signal H_b decays, an extended maximum likelihood fit is performed to the Λ_b^0, Ξ_b^0, and Ξ_b^- invariant-mass spectra. A kinematic refit [27] is applied to the H_b decays to improve the mass resolution, constraining the D_s^- and H_c masses to their previously measured values [2] and the H_b momentum to point back to its PV. The fitted mass region is 5450 – 5800 MeV/c^2, 5600 – 6100 MeV/c^2, and 5600 – 6000 MeV/c^2 for the Λ_b^0, Ξ_b^0, and Ξ_b^- decays, respectively.

As shown in Fig. 1, three components are identified in each H_b mass spectrum. The signal component is parameterised using the sum of a Gaussian and a double-sided Crystal Ball function (DSCB) [28] sharing a common mean. The common mean and the average resolution of the Gaussian and the DSCB distribution are parameters that vary freely in the fit, while the other parameters have values fixed to those obtained from simulation. The contribution of combinatorial backgrounds in the mass spectrum is modelled using a second order polynomial, with all parameters varying freely. The peaking structure in the low invariant-mass region corresponds to partially reconstructed $H_b \rightarrow H_c D_s^- X$

decays where X is an undetected particle. Distributions from data in the low mass region are found to be consistent with the $H_b \to H_c D_s^{*-}$, $D_s^{*-} \to D_s^- \gamma$ sequential decay, where the γ is not reconstructed. The subsequent $H_c D_s^-$ invariant-mass distribution depends on the D_s^{*-} helicity projection, for which three possibilities, helicities of ± 1 and 0, are allowed. The mass distributions for helicities of $+1$ and -1 are identical. Samples are generated with helicities of 1 and 0, and corresponding $H_c D_s^-$ invariant-mass distributions are obtained. The distributions convoluted with experimental resolutions are used to fit data. The fraction of the component with a helicity of 0 varies freely in the fit.

Figure 1 shows the H_b invariant-mass distributions superimposed by the fit results. The signal yields for Λ_b^0, Ξ_b^0 and Ξ_b^- decays are $(2.609 \pm 0.017) \times 10^4$, 462 ± 29, and 175 ± 14, respectively. The masses for Λ_b^0, Ξ_b^0 and Ξ_b^- baryons are measured to be $m_{\Lambda_b^0} = 5619.34 \pm 0.06\,\mathrm{MeV}/c^2$, $m_{\Xi_b^0} = 5791.12 \pm 0.60\,\mathrm{MeV}/c^2$, and $m_{\Xi_b^-} = 5797.02 \pm 0.63\,\mathrm{MeV}/c^2$, respectively, where the uncertainties are statistical only.

4.1 Non-dicharm background

The sample of $H_b \to H_c D_s$ decays is polluted by beauty-baryon decays that have the same final-state particles but do not decay through the two intermediate charmed hadrons, H_c or D_s^-, we are investigating. These are referred to as non-dicharm decays. For these peaking background contributions, their H_b invariant-mass distributions are signal-like, but the invariant-mass distributions of H_c and/or D_s^- candidates are flat. The distributions of non-dicharm components in the H_c or D_s^- invariant-mass distribution are found to be approximately linear. Therefore, the H_b signal yields in the H_c and D_s^- sideband regions are extrapolated to the signal region ($\pm 25\,\mathrm{MeV}/c^2$ around the previously measured H_c and D_s^- masses [2]) to estimate the contamination of non-dicharm background in the signal region. Details of the estimation are shown in Appendix A. The fractions of non-dicharm decays are measured to be $(5.70 \pm 0.13)\%$, $(8.39 \pm 1.75)\%$ and $(6.44 \pm 1.48)\%$ for Λ_b^0, Ξ_b^0 and Ξ_b^- decays, respectively. These background contributions are subtracted from the total signal yield obtained from the fit. The non-dicharm contamination is dominated by the $H_b \to H_c(K^+K^-\pi^-)$ component.

5 Systematic uncertainties

5.1 Uncertainties on the branching fraction

Measurements of the ratios of branching fractions are affected by a number of systematic uncertainties. Apart from those due to the input charmed-decay branching fractions, they are generally related to either the signal yields or the efficiencies. Due to the similar topologies of the three H_b decays, many sources of systematic uncertainties are either cancelled or largely suppressed in ratios of the branching fractions. The remaining systematic uncertainties are outlined below and summarised in Table 2.

5.1.1 Systematic uncertainties on the signal yield

The fit results are affected by the imperfect modelling of the signal, the combinatorial background and the partially reconstructed background. Variations of the signal model are studied by changing the fixed value of the fraction of Gaussian component to 0.0 and two times of the nominal value, respectively. For the background modelling, a polynomial of third order is used instead of one of second order. In order to study the impact of the modelling of the partially reconstructed background in the signal yield, the lower edge of the fit range is increased to 5575, 5740, and 5750 MeV/c^2 for the Λ_b^0, Ξ_b^0, and Ξ_b^- decay modes, respectively, excluding partially reconstructed background. Alternative fits to data with these alternate approaches are performed. The largest deviation of the H_b signal yield in these alternative fits from the nominal result is taken as the systematic uncertainty on the signal yield due to the modelling of the fit components, which is at the level of 2%.

The uncertainty on the fraction of non-dicharm background discussed in Sect. 4.1 originates from the limited size of the data sample and possible nonlinearity of the H_c and D_s^- background invariant-mass distributions. The effect is studied by using alternative regions of sideband data to calculate the non-dicharm yield, and the difference with respect to the nominal results is quoted as the systematic uncertainty, which is found to be at the subpercent level.

5.1.2 Systematic uncertainties on the efficiency

As efficiencies are studied using simulation samples, the systematic uncertainty on efficiencies arises due to the limited size of simulation samples and imperfect simulations. The uncertainty due to the limited simulation sample size is 1.0% for the three H_b efficiency ratios.

The hardware trigger is approximately modeled in the simulation. The trigger efficiency in measured in the data [29], and the difference between data and simulation is assigned as a systematic uncertainty. This systematic uncertainty is found to be approximately cancelled among the three H_b decay modes, resulting in a relative difference of less than 1.5% between data and simulation on the efficiency ratios of the two H_b decay modes. A common value of 1.5% is quoted as the relative systematic uncertainty of the hardware trigger on the relative branching fraction.

Table 2 Systematic uncertainties on the relative branching fraction measurements. Results are given as relative uncertainties

Source	$\mathcal{R}\left(\frac{\Xi_b^0}{\Lambda_b^0}\right)$	$\mathcal{R}\left(\frac{\Xi_b^-}{\Lambda_b^0}\right)$	$\mathcal{R}\left(\frac{\Xi_b^0}{\Xi_b^-}\right)$
Imperfect modelling of invariant-mass fit	2.7%	1.3%	3.4%
Fraction of non-dicharm background	2.0%	1.6%	2.5%
Limited simulation sample size	0.9%	1.0%	0.8%
Trigger efficiency	1.5%	1.5%	1.5%
Reconstruction efficiency	0.1%	1.6%	1.7%
Corrections to simulations	1.3%	4.3%	4.3%
Total	4.0%	5.4%	6.5%

The estimation of the reconstruction efficiency is affected by the model of detector material in simulation which affects the description of interaction between the final-state particles and the material. It leads to a relative uncertainty of 1.2% between Ξ_b^- and the other two H_b decays due to one additional kaon in the Ξ_b^- decay [30]. Moreover, the estimation of the track-finding efficiency in data and simulation is subjected to uncertainties related to the detector occupancy and limited sizes of the calibration samples [25]. The former gives a relative value of 0.8% per track, while the latter results in an uncertainty of around 0.1% on the efficiency ratios. In total the uncertainty on the ratio of reconstruction efficiency is about 1.6% between Ξ_b^- and Λ_b^0 decays, and between Ξ_b^0 and Ξ_b^- decays. It is below 0.1% for the efficiency ratio between Ξ_b^0 and Λ_b^0 decays.

Corrections to simulation samples to match data to the distributions of final-state particle PID responses, H_b kinematics, charged-track multiplicity and H_c Dalitz distributions are subject to uncertainties. Uncertainties on the corrections of PID responses are evaluated using alternative corrections and measuring the relative change of efficiencies [22], which is found to be negligible. The uncertainty on corrections of H_b kinematics is studied with pseudoexperiments. For each pesudoexperiment, the correction factor in each transverse momentum and rapidity of the H_b baryon is varied following a Gaussian distribution constructed from the nominal value and its uncertainty. The new correction factors are used to calculate the efficiency. The width of the efficiency distribution among a set of pseudoexperiments is taken as the systematic uncertainty. Similar studies are performed for corrections of the charge-track multiplicity and Λ_c^+, Ξ_c^+ Dalitz distributions. The uncertainty of the unbinned correction to the Ξ_c^0 Dalitz distribution is studied by varying the configurations of the algorithm [26]. In total the uncertainty on the efficiency ratio originating from corrections to simulation samples is about 4.3% between Ξ_b^- and Λ_b^0, 4.3% between Ξ_b^0 and Ξ_b^-, and 1.3% between Ξ_b^0 and Λ_b^0.

5.2 Uncertainties on the H_b mass measurements

The uncertainties on the mass and mass difference measurements come from the invariant-mass fit model, the momentum scale calibration, and the uncertainties on the Ξ_c and D_s^- masses [2]. They are summarised in Tables 3 and 4.

The H_b mass determined from the fit to the invariant-mass distribution is affected by the imperfect modelling of the signal, the combinatorial background and the partially reconstructed background. Variations of the model for each fit component are studied in the same way as for the determination of the uncertainties on the signal yield described in Sect. 5.1.1. The largest variation of the mass obtained in these alternative fits compared to the nominal one is considered as the systematic uncertainty, which is 0.02, 0.19 and 0.09 MeV/c^2 for $m_{\Lambda_b^0}$, $m_{\Xi_b^0}$ and $m_{\Xi_b^-}$, respectively. The larger uncertainty for $m_{\Xi_b^0}$ is due to the higher background level.

Due to effects such as an imperfect alignment of the tracking system and the uncertainty on the magnetic field, the measured track momenta need to be calibrated to correct for possible biases. The calibration is performed using the masses of known hadrons [31,32] with a precision of 0.03%. The uncertainty is propagated to the H_b mass measurement by varying the calibration by ± 1 standard deviation. Half of the difference between the two corresponding new H_b masses is taken as the systematic uncertainty. The result, about 0.4 MeV/c^2, approximately scales with the energy release of the decay as $(m(H_b) - m(H_c) - m(D_s^-)) \times 0.03\%$. The uncertainty due to momentum scale calibration is assumed to be fully correlated for the three H_b masses.

As mentioned in Sect. 4, the H_b invariant mass is calculated with the D_s^- and H_c masses constrained to their previous world averages [2]. The systematic uncertainty due to the H_c and D_s^- masses is 0.16, 0.24, and 0.29 MeV/c^2 for the Λ_b^0, Ξ_b^0, and Ξ_b^- mass measurement, respectively. When measuring the mass difference between two different H_b states, the uncertainty on the D_s^- mass is cancelled. The remaining uncertainty on the H_c mass varies between 0.23 and 0.31 MeV/c^2 depending on mass difference.

Table 3 Systematic uncertainties for the H_b mass measurements

Source	$m_{\Lambda_b^0}$ [MeV/c^2]	$m_{\Xi_b^0}$ [MeV/c^2]	$m_{\Xi_b^-}$ [MeV/c^2]
Mass fit model	0.02	0.19	0.09
Momentum scale calibration	0.44	0.41	0.48
Uncertainties on the H_c and D_s^- masses	0.16	0.24	0.29

Table 4 Systematic uncertainties for the H_b mass-difference measurements

Source	$m_{\Xi_b^0} - m_{\Lambda_b^0}$ [MeV/c^2]	$m_{\Xi_b^-} - m_{\Lambda_b^0}$ [MeV/c^2]	$m_{\Xi_b^-} - m_{\Xi_b^0}$ [MeV/c^2]
Mass fit model	0.19	0.09	0.21
Momentum scale calibration	0.03	0.04	0.07
Uncertainties on the H_c mass	0.27	0.31	0.23

Table 5 Measured H_b masses and mass differences and the previous world averages [2]

	This analysis [MeV/c^2]	Previous world average [MeV/c^2]
$m_{\Lambda_b^0}$	5619.34 ± 0.47	5619.60 ± 0.17
$m_{\Xi_b^0}$	5791.1 ± 0.8	5791.9 ± 0.5
$m_{\Xi_b^-}$	5797.0 ± 0.8	5797.0 ± 0.6
$m_{\Xi_b^0} - m_{\Lambda_b^0}$	171.8 ± 0.7	172.5 ± 0.4
$m_{\Xi_b^-} - m_{\Lambda_b^0}$	177.7 ± 0.7	177.46 ± 0.31
$m_{\Xi_b^-} - m_{\Xi_b^0}$	5.9 ± 0.9	5.9 ± 0.6

6 Results

Using the results presented in the previous sections, the H_b masses and mass differences are measured to be

$$m_{\Lambda_b^0} = 5619.34 \pm 0.06 \pm 0.44 \pm 0.16 \,\mathrm{MeV}/c^2,$$

$$m_{\Xi_b^0} = 5791.12 \pm 0.60 \pm 0.45 \pm 0.24 \,\mathrm{MeV}/c^2,$$

$$m_{\Xi_b^-} = 5797.02 \pm 0.63 \pm 0.49 \pm 0.29 \,\mathrm{MeV}/c^2,$$

$$m_{\Xi_b^0} - m_{\Lambda_b^0} = 171.78 \pm 0.60 \pm 0.19 \pm 0.27 \,\mathrm{MeV}/c^2,$$

$$m_{\Xi_b^-} - m_{\Lambda_b^0} = 177.68 \pm 0.63 \pm 0.10 \pm 0.31 \,\mathrm{MeV}/c^2,$$

$$m_{\Xi_b^-} - m_{\Xi_b^0} = 5.90 \pm 0.87 \pm 0.22 \pm 0.23 \,\mathrm{MeV}/c^2,$$

where the first uncertainties are statistical, the second systematic, and the third due to those on masses of Λ_c^+, Ξ_c^+, Ξ_c^0, and D_s^- hadrons. The measurements are consistent with previous world averages [2], and comparisons are shown in Table 5 and Fig. 2.

The relative production rates of the three $H_b \rightarrow H_c D_s$ decays, given in Eqs. (1)–(3), are measured to be

$$\mathcal{R}\left(\frac{\Xi_b^0}{\Lambda_b^0}\right) = (15.8 \pm 1.1 \pm 0.6 \pm 7.7)\%,$$

$$\mathcal{R}\left(\frac{\Xi_b^-}{\Lambda_b^0}\right) = (16.9 \pm 1.3 \pm 0.9 \pm 4.3)\%,$$

$$\mathcal{R}\left(\frac{\Xi_b^0}{\Xi_b^-}\right) = (93.6 \pm 9.6 \pm 6.1 \pm 51.0)\%,$$

where the first uncertainties are statistical, the second systematic, and the third due to those on the branching fractions of Λ_c^+, Ξ_c^+, and Ξ_c^0 decays. Figure 3 shows the measured $\mathcal{R}$ values. The results are consistent with the $SU(3)$ flavour symmetry and predictions of phenomenological models [33,34].

7 Summary

In this analysis, the dicharm decays of Ξ_b baryons $\Xi_b^0 \rightarrow \Xi_c^+ D_s^-$ and $\Xi_b^- \rightarrow \Xi_c^0 D_s^-$ are observed for the first time.

Fig. 2 Comparison of measured (red) b baryon masses with (blue) the PDG values [2]. The mass of Λ_b^0 is shifted upward by 175 MeV/c^2 to reduce the range of this plot. The inner (outer) error bar is for the statistical (total) uncertainty
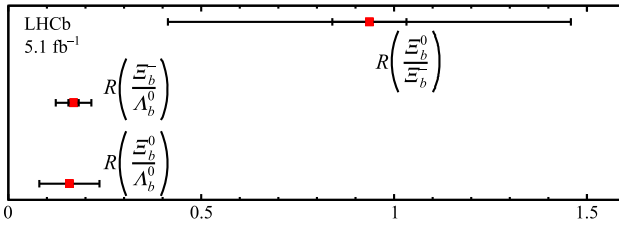
Fig. 3 Measured $\mathcal{R}$ values. The inner (outer) error bar is for the statistical (total) uncertainty

The data sample is the proton-proton collision data collected by the LHCb experiment at a centre-of-mass energy of $\sqrt{s} = 13$ TeV and corresponding to an integrated luminosity of 5.1 fb^{-1}. The masses of the Λ_b^0, Ξ_b^0 and Ξ_b^- baryons are measured through these two decays, and are consistent with the previous world average values [2]. These measurements will improve the world averages. The relative branching fractions of these two decays are also measured. The results are consistent with $SU(3)$ flavour symmetry and several predictions for relative production rates and decay branching fractions of b baryons [6,33–35].

Data availability statement The manuscript has associated data in a data repository. [Authors' comment: All LHCb scientific output is published in journals, with preliminary results made available in Conference Reports. All are Open Access, without restriction on use beyond the standard conditions agreed by CERN. Data associated to the plots in this publication as well as in supplementary materials are made available on the CERN document server at http://cdsweb.cern.ch/record/. This information is taken from the LHCb External Data Access Policy which can be downloaded at http://opendata.cern.ch/record/410].

Appendices

A Non-dicharm contribution

Three distinct sources of non-dicharm backgrounds are considered:

- The $H_b \to (pK^-(K^-)\pi^+)(K^+K^-\pi^+)$ decay with neither the H_c nor the D_s^- hadrons.
- The $H_b \to (pK^-(K^-)\pi^+)D_s^-$ decay without the H_c baryon.
- The $H_b \to H_c(K^+K^-\pi^+)$ decay without the D_s^- meson.

Figure 4 shows the two-dimensional H_c versus D_s^- invariant-mass distribution in the signal region and the H_c and/or D_s^- sideband regions. There are four regions illustrated in Fig. 4:

- The region 1 lies in the H_c and D_s^- sideband region.
- The region 2 lies in the H_c signal and D_s^- sideband region.
- The region 3 lies in the H_c sideband and D_s^- signal region.
- The region 4 lies in the H_c and D_s^- signal region.

The $H_b \to (pK^-(K^-)\pi^+)(K^+K^-\pi^+)$ decay populates every region, the $H_b \to (pK^-(K^-)\pi^+)D_s^-$ decay populates regions 2 and 4, the $H_b \to (pK^-(K^-)\pi^+)D_s^-$ decay only populates regions 3 and 4, and real signal only populates region 4. Besides, the distributions of non-dicharm components in the H_c or D_s^- invariant-mass distribution are found to be approximately linear. Thus, the number of non-dicharm backgrounds in region 4 can be calculated as

$$N_{\text{non-dicharm}} = 0.5 \times (N_2 + N_3) - 0.25 \times N_1, \qquad (7)$$

where N_1, N_2 and N_3 are the H_b yields in region 1, 2, and 3, respectively. N_1, N_2 and N_3 are estimated by simultaneous fitting to the H_b invariant-mass spectra in these regions. The fit model is similar as the one mentioned in Sect. 4. Figures 5, 6, and 7 show the Λ_b^0, Ξ_b^0, and Ξ_b^- invariant-mass distributions in the H_c and/or D_s^- sideband regions superimposed by the fit results, respectively.
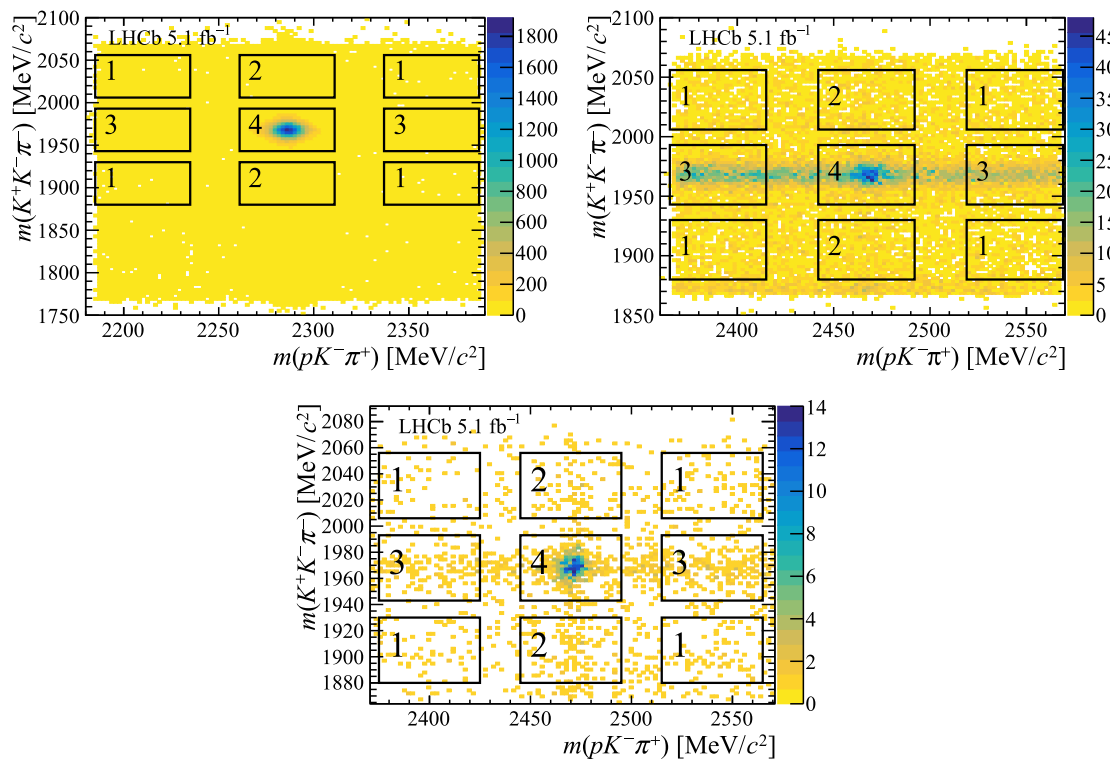
Fig. 4 Distributions of the H_c mass versus the D_s^- mass with the regions 1–4 indicated for (top left) Λ_b^0, (top right) Ξ_b^0, and (bottom) Ξ_b^- mode. The region 1 lies in the H_c and D_s^- sideband region. The region 2 lies in the H_c signal and D_s^- sideband region. The region 3 lies in the H_c sideband and D_s^- signal region. The region 4 lies in the H_c and D_s^- signal region
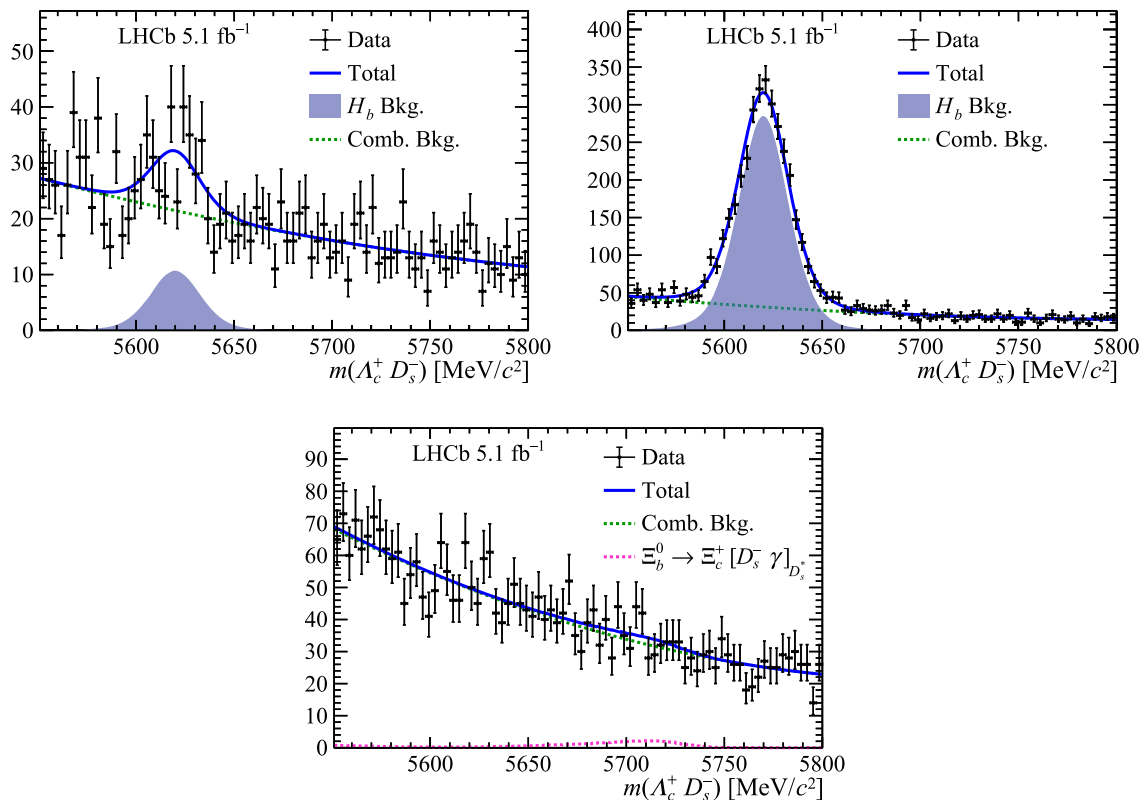
Fig. 5 Invariant-mass distributions of Λ_b^0 candidates in the (top left) region 1, (top right) region 2, and (bottom) region 3
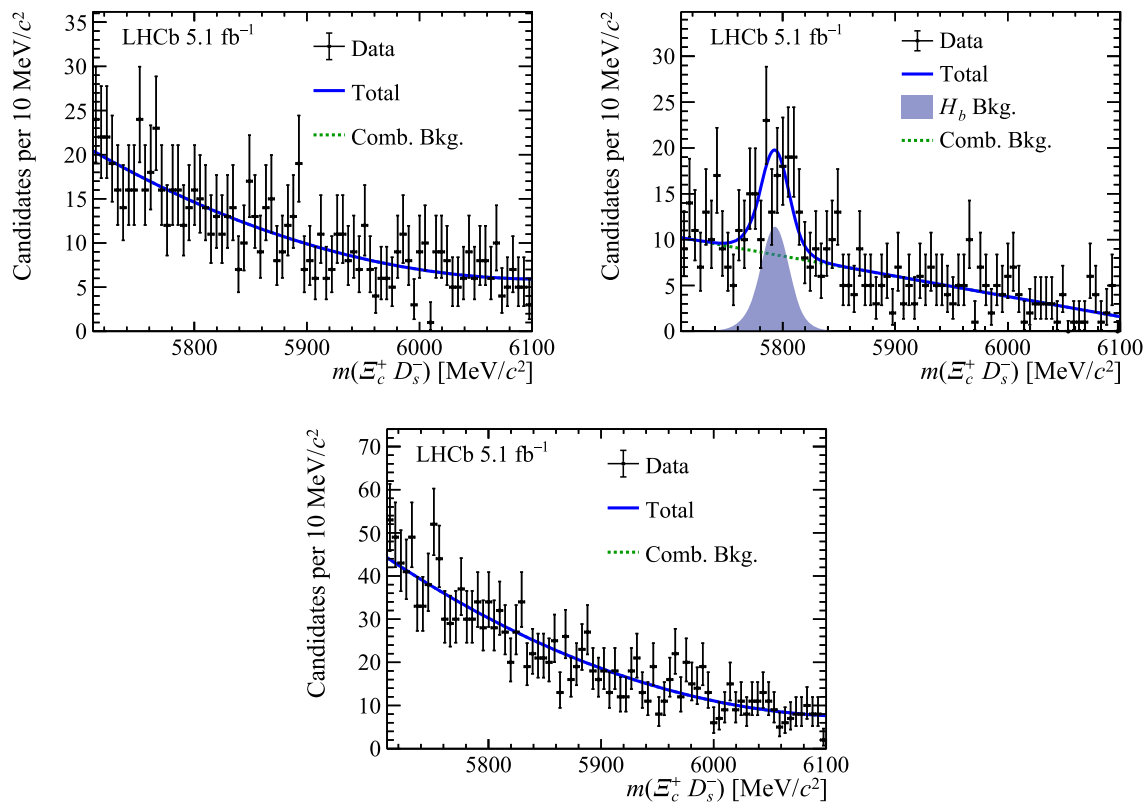
Fig. 6 Invariant-mass distributions of Λ_b^0 candidates in the (top left) region 1, (top right) region 2, and (bottom) region 3
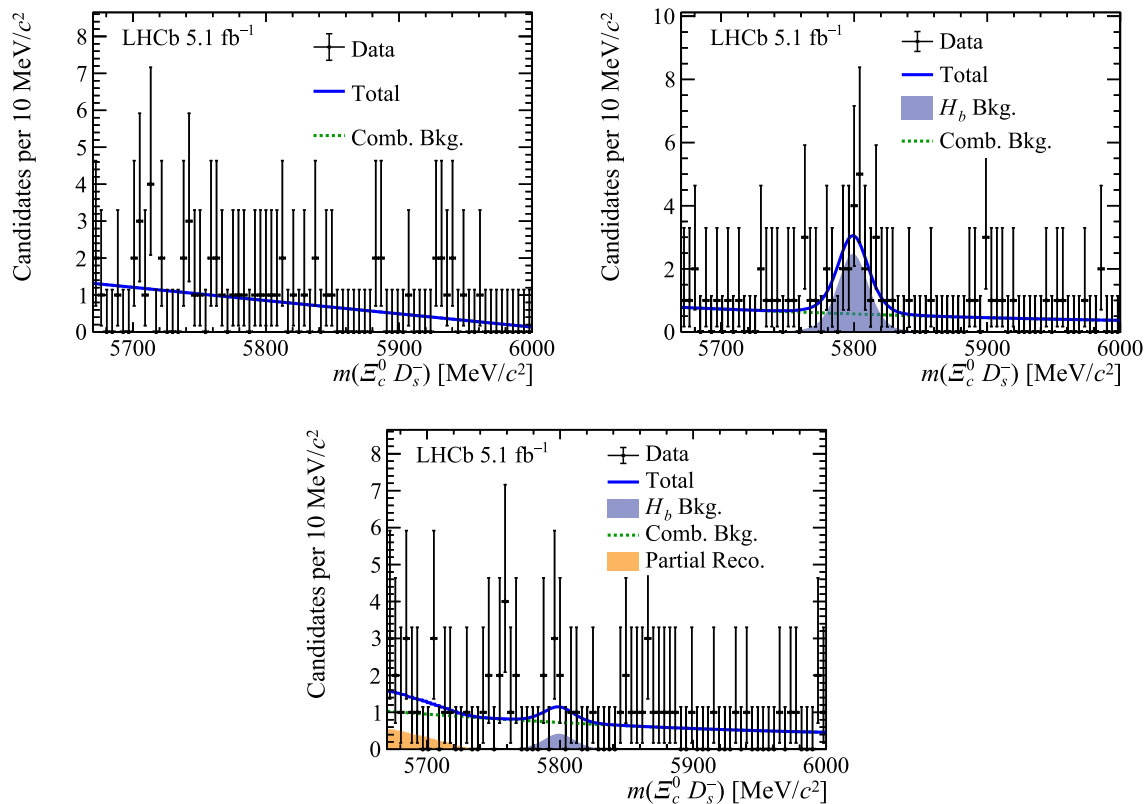
Fig. 7 Invariant-mass distributions of Λ_b^0 candidates in the (top left) region 1, (top right) region 2, and (bottom) region 3

References

1. S. Chen et al., Heavy flavour physics and CP violation at LHCb: a ten-year review. Front. Phys. **18**, 44601 (2023). https://doi.org/10.1007/s11467-022-1247-1. arXiv:2111.14360

2. Particle Data Group, R. L. Workman et al., Review of particle physics, Prog. Theor. Exp. Phys. **2022**, 083C01 (2022). https://doi.org/10.1093/ptep/ptac097. http://pdg.lbl.gov/

3. A. Lenz, Lifetimes and heavy quark expansion. Int. J. Mod. Phys. A **30**, 1543005 (2015). https://doi.org/10.1142/S0217751X15430058. arXiv:1405.3601

4. M. Neubert, B decays and the heavy quark expansion. Adv. Ser. Direct. High Energy Phys. **15**, 239 (1998). https://doi.org/10.1142/9789812812667_0003. arXiv:hep-ph/9702375

5. M. Neubert, Heavy quark symmetry. Phys. Rept. **245**, 259 (1994). https://doi.org/10.1016/0370-1573(94)90091-4. arXiv:hep-ph/9306320

6. C.-K. Chua, Color-allowed bottom baryon to s-wave and p-wave charmed baryon nonleptonic decays. Phys. Rev. D **100**, 034025 (2019). https://doi.org/10.1103/PhysRevD.100.034025. arXiv:1905.00153

7. LHCb collaboration, R. Aaij et al., Study of beauty hadron decays into pairs of charm hadrons. Phys. Rev. Lett. **112**, 202001 (2014). https://doi.org/10.1103/PhysRevLett.112.202001. arXiv:1403.3606

8. LHCb collaboration, R. Aaij et al., Measurement of b hadron production fractions in 7TeV pp collisions. Phys. Rev. D **85**, 032008 (2012). https://doi.org/10.1103/PhysRevD.85.032008. arXiv:1111.2357

9. LHCb collaboration, R. Aaij et al., Study of the kinematic dependences of Λ_b^0 production in pp collisions and a measurement of the $\Lambda_b^0 \to \Lambda_c^+ \pi^-$ branching fraction. JHEP **08**, 143 (2014). https://doi.org/10.1007/JHEP08(2014)143. arXiv:1405.6842

10. LHCb collaboration, R. Aaij et al., Measurement of b-hadron fractions in 13TeV pp collisions. Phys. Rev. D **100**, 031102(R) (2019). https://doi.org/10.1103/PhysRevD.100.031102. arXiv:1902.06794

11. LHCb collaboration, R. Aaij et al., Measurement of the mass and production rate of Ξ_b^- baryons. Phys. Rev. D **99**, 052006 (2019). https://doi.org/10.1103/PhysRevD.99.052006. arXiv:1901.07075

12. LHCb collaboration, R. Aaij et al., LHCb detector performance. Int. J. Mod. Phys. A **30**, 1530022 (2015). https://doi.org/10.1142/S0217751X15300227. arXiv:1412.6352

13. LHCb collaboration, A. A. Alves Jr. et al., The LHCb detector at the LHC, JINST **3**, S08005 (2008). https://doi.org/10.1088/1748-0221/3/08/S08005

14. LHCb collaboration, R. Aaij et al., Measurement of the Λ_b^0, Ξ_b^- and Ω_b^- baryon masses. Phys. Rev. Lett. **110**, 182001 (2013). https://doi.org/10.1103/PhysRevLett.110.182001. arXiv:1302.1072

15. LHCb collaboration, R. Aaij et al., Precision measurement of D meson mass differences. JHEP **06**, 065 (2013). https://doi.org/10.1007/JHEP06(2013)065. arXiv:1304.6865

16. R. Aaij et al., Performance of the LHCb trigger and full real-time reconstruction in Run 2 of the LHC. JINST **14**, P04013 (2019). https://doi.org/10.1088/1748-0221/14/04/P04013. arXiv:1812.10790

17. T. Sjöstrand, S. Mrenna, and P. Skands, A brief introduction to PYTHIA 8.1. Comput. Phys. Commun. **178**, 852 (2008). https://doi.org/10.1016/j.cpc.2008.01.036. arXiv:0710.3820

18. D.J. Lange, The EvtGen particle decay simulation package. Nucl. Instrum. Meth. **A462**, 152 (2001). https://doi.org/10.1016/S0168-9002(01)00089-4

19. N. Davidson, T. Przedzinski, and Z. Was, PHOTOS interface in C++: Technical and physics documentation. Comp. Phys. Comm. **199**, 86 (2016). https://doi.org/10.1016/j.cpc.2015.09.013. arXiv:1011.0937

20. Geant4 collaboration, J. Allison et al., Geant4 developments and applications. IEEE Trans. Nucl. Sci. **53**, 270 (2006). https://doi.org/10.1109/TNS.2006.869826

21. LHCb collaboration, M. Clemencic et al., The LHCb simulation application, Gauss: Design, evolution and experience. J. Phys. Conf. Ser. **331**, 032023 (2011). https://doi.org/10.1088/1742-6596/331/3/032023

22. R. Aaij et al., Selection and processing of calibration samples to measure the particle identification performance of the LHCb experiment in Run 2. Eur. Phys. J. Tech. Instr. **6**, 1 (2019). https://doi.org/10.1140/epjti/s40485-019-0050-z. arXiv:1803.00824

23. Y. Freund, R.E. Schapire, A decision-theoretic generalization of on-line learning and an application to boosting. J. Comput. Syst. Sci. **55**, 119 (1997). https://doi.org/10.1006/jcss.1997.1504

24. R.H. Dalitz, On the analysis of τ-meson data and the nature of the τ-meson. Phil. Mag. Ser. 7 **44**, 1068 (1953). https://doi.org/10.1080/14786441008520365

25. LHCb collaboration, R. Aaij et al., Measurement of the track reconstruction efficiency at LHCb. JINST **10**, P02007 (2015). https://doi.org/10.1088/1748-0221/10/02/P02007. arXiv:1408.1251

26. A. Rogozhnikov, Reweighting with boosted decision trees. J. Phys. Conf. Ser. **762**, 012036 (2016). https://doi.org/10.1088/1742-6596/762/1/012036. arXiv:1608.05806

27. W.D. Hulsbergen, Decay chain fitting with a Kalman filter. Nucl. Instrum. Meth. **A552**, 566 (2005). https://doi.org/10.1016/j.nima.2005.06.078. arXiv:physics/0503191

28. T. Skwarnicki, A study of the radiative cascade transitions between the Upsilon-prime and Upsilon resonances, PhD thesis, Institute of Nuclear Physics, Krakow, (1986), http://inspirehep.net/record/230779/DESY-F31-86-02

29. C. Abellan Beteta et al., Calibration and performance of the LHCb calorimeters in Run 1 and 2 at the LHC. arXiv:2008.11556, submitted to JINST

30. LHCb collaboration, R. Aaij et al., Measurement of the track reconstruction efficiency at LHCb. JINST **10**, P02007 (2015). https://doi.org/10.1088/1748-0221/10/02/P02007. arXiv:1408.1251

31. LHCb collaboration, R. Aaij et al., Measurement of b-hadron masses. Phys. Lett. B **708**, 241 (2012). https://doi.org/10.1016/j.physletb.2012.01.058. arXiv:1112.4896

32. LHCb collaboration, R. Aaij et al., Precision measurement of D meson mass differences. JHEP **06**, 065 (2013). https://doi.org/10.1007/JHEP06(2013)065. arXiv:1304.6865

33. Y.K. Hsiao, P.Y. Lin, L.W. Luo, C.Q. Geng, Fragmentation fractions of two-body b-baryon decays. Phys. Lett. B **751**, 127 (2015). https://doi.org/10.1016/j.physletb.2015.10.013. arXiv:1510.01808

34. H.-Y. Jiang, F.-S. Yu, Fragmentation-fraction ratio f_{Ξ_b}/f_{Λ_b} in b- and c-baryon decays. Eur. Phys. J. C **78**, 224 (2018). https://doi.org/10.1140/epjc/s10052-018-5704-5. arXiv:1802.02948

35. Y.-S. Li, X. Liu, Restudy of the color-allowed two-body nonleptonic decays of bottom baryons Ξb and Ωb supported by hadron spectroscopy. Phys. Rev. D **105**, 013003 (2022). https://doi.org/10.1103/PhysRevD.105.013003. arXiv:2112.02481

LHCb collaboration

R. Aaij[33], A. S. W. Abdelmotteleb[52], C. Abellan Beteta[46], F. Abudinén[52], T. Ackernley[56], B. Adeva[42], M. Adinolfi[50], P. Adlarson[78], H. Afsharnia[10], C. Agapopoulou[44], C. A. Aidala[79], Z. Ajaltouni[10], S. Akar[61], K. Akiba[33], P. Albicocco[24], J. Albrecht[16], F. Alessio[44], M. Alexander[55], A. Alfonso Albero[41], Z. Aliouche[58], P. Alvarez Cartelle[51], R. Amalric[14], S. Amato[2], J. L. Amey[50], Y. Amhis[12,44], L. An[5], L. Anderlini[23], M. Andersson[46], A. Andreianov[39], P. Andreola[46], M. Andreotti[22], D. Andreou[64], D. Ao[6], F. Archilli[32,v], S. Arguedas Cuendis[8], A. Artamonov[39], M. Artuso[64], E. Aslanides[11], M. Atzeni[60], B. Audurier[13], D. Bacher[59], I. Bachiller Perea[9], S. Bachmann[18], M. Bachmayer[45], J. J. Back[52], A. Bailly-reyre[14], P. Baladron Rodriguez[42], V. Balagura[13], W. Baldini[22,44], J. Baptista de Souza Leite[1], M. Barbetti[23,m], I. R. Barbosa[66], R. J. Barlow[58], S. Barsuk[12], W. Barter[54], M. Bartolini[51], F. Baryshnikov[39], J. M. Basels[15], G. Bassi[30,s], B. Batsukh[4], A. Battig[16], A. Bay[45], A. Beck[52], M. Becker[16], F. Bedeschi[30], I. B. Bediaga[1], A. Beiter[64], S. Belin[42], V. Bellee[46], K. Belous[39], I. Belov[25], I. Belyaev[39], G. Benane[11], G. Bencivenni[24], E. Ben-Haim[14], A. Berezhnoy[39], R. Bernet[46], S. Bernet Andres[40], D. Berninghoff[18], H. C. Bernstein[64], C. Bertella[58], A. Bertolin[29], C. Betancourt[46], F. Betti[54], J. Bex[51], Ia. Bezshyiko[46], J. Bhom[36], L. Bian[70], M. S. Bieker[16], N. V. Biesuz[22], P. Billoir[14], A. Biolchini[33], M. Birch[57], F. C. R. Bishop[51], A. Bitadze[58], A. Bizzeti, M. P. Blago[51], T. Blake[52], F. Blanc[45], J. E. Blank[16], S. Blusk[64], D. Bobulska[55], V. Bocharnikov[39], J. A. Boelhauve[16], O. Boente Garcia[13], T. Boettcher[61], A. Bohare[54], A. Boldyrev[39], C. S. Bolognani[76], R. Bolzonella[22,l], N. Bondar[39], F. Borgato[29,44], S. Borghi[58], M. Borsato[18], J. T. Borsuk[36], S. A. Bouchiba[45], T. J. V. Bowcock[56], A. Boyer[44], C. Bozzi[22], M. J. Bradley[57], S. Braun[62], A. Brea Rodriguez[42], N. Breer[16], J. Brodzicka[36], A. Brossa Gonzalo[42], J. Brown[56], D. Brundu[28], A. Buonaura[46], L. Buonincontri[29], A. T. Burke[58], C. Burr[44], A. Bursche[68], A. Butkevich[39], J. S. Butter[33], J. Buytaert[44], W. Byczynski[44], S. Cadeddu[28], H. Cai[70], R. Calabrese[22,l], L. Calefice[16], S. Cali[24], M. Calvi[27,p], M. Calvo Gomez[40], J. Cambon Bouzas[42], P. Campana[24], D. H. Campora Perez[76], A. F. Campoverde Quezada[6], S. Capelli[27,p], L. Capriotti[22], A. Carbone[21,j], L. Carcedo Salgado[42], R. Cardinale[25,n], A. Cardini[28], P. Carniti[27,p], L. Carus[18], A. Casais Vidal[42], R. Caspary[18], G. Casse[56], M. Cattaneo[44], G. Cavallero[22], V. Cavallini[22,l], S. Celani[45], J. Cerasoli[11], D. Cervenkov[59], S. Cesare[26,o], A. J. Chadwick[56], I. Chahrour[79], M. G. Chapman[50], M. Charles[14], Ph. Charpentier[44], C. A. Chavez Barajas[56], M. Chefdeville[9], C. Chen[11], S. Chen[4], A. Chernov[36], S. Chernyshenko[48], V. Chobanova[42,z], S. Cholak[45], M. Chrzaszcz[36], A. Chubykin[39], V. Chulikov[39], P. Ciambrone[24], M. F. Cicala[52], X. Cid Vidal[42], G. Ciezarek[44], P. Cifra[44], P. E. L. Clarke[54], M. Clemencic[44], H. V. Cliff[51], J. Closier[44], J. L. Cobbledick[58], C. Cocha Toapaxi[18], V. Coco[44], J. Cogan[11], E. Cogneras[10], L. Cojocariu[38], P. Collins[44], T. Colombo[44], A. Comerma-Montells[41], L. Congedo[20], A. Contu[28], N. Cooke[55], I. Corredoira[42], A. Correia[14], G. Corti[44], J. J. Cottee Meldrum[50], B. Couturier[44], D. C. Craik[46], M. Cruz Torres[1,h], R. Currie[54], C. L. Da Silva[63], S. Dadabaev[39], L. Dai[67], X. Dai[5], E. Dall'Occo[16], J. Dalseno[42], C. D'Ambrosio[44], J. Daniel[10], A. Danilina[39], P. d'Argent[20], A. Davidson[52], J. E. Davies[58], A. Davis[58], O. De Aguiar Francisco[58], C. De Angelis[28,k], J. de Boer[33], K. De Bruyn[75], S. De Capua[58], M. De Cian[18], U. De Freitas Carneiro Da Graca[1,b], E. De Lucia[24], J. M. De Miranda[1], L. De Paula[2], M. De Serio[20,i], D. De Simone[46], P. De Simone[24], F. De Vellis[16], J. A. de Vries[76], C. T. Dean[63], F. Debernardis[20,i], D. Decamp[9], V. Dedu[11], L. Del Buono[14], B. Delaney[60], H.-P. Dembinski[16], J. Deng[7], V. Denysenko[46], O. Deschamps[10], F. Dettori[28,k], B. Dey[73], P. Di Nezza[24], I. Diachkov[39], S. Didenko[39], S. Ding[64], V. Dobishuk[48], A. D. Docheva[55], A. Dolmatov[39], C. Dong[3], A. M. Donohoe[19], F. Dordei[28], A. C. dos Reis[1], L. Douglas[55], A. G. Downes[9], W. Duan[68], P. Duda[77], M. W. Dudek[36], L. Dufour[44], V. Duk[74], P. Durante[44], M. M. Duras[77], J. M. Durham[63], D. Dutta[58], A. Dziurda[36], A. Dzyuba[39], S. Easo[53,44], E. Eckstein[72], U. Egede[65], A. Egorychev[39], V. Egorychev[39], C. Eirea Orro[42], S. Eisenhardt[54], E. Ejopu[58], S. Ek-In[45], L. Eklund[78], M. Elashri[61], J. Ellbracht[16], S. Ely[57], A. Ene[38], E. Epple[61], S. Escher[15], J. Eschle[46], S. Esen[46], T. Evans[58], F. Fabiano[28,k,44], L. N. Falcao[1], Y. Fan[6], B. Fang[70,12], L. Fantini[74,r], M. Faria[45], K. Farmer[54], S. Farry[56], D. Fazzini[27,p], L. Felkowski[77], M. Feng[4,6], M. Feo[44], M. Fernandez Gomez[42], A. D. Fernez[62], F. Ferrari[21], L. Ferreira Lopes[45], F. Ferreira Rodrigues[2], S. Ferreres Sole[33], M. Ferrillo[46], M. Ferro-Luzzi[44], S. Filippov[39], R. A. Fini[20], M. Fiorini[22,l], M. Firlej[35], K. M. Fischer[59], D. S. Fitzgerald[79], C. Fitzpatrick[58], T. Fiutowski[35], F. Fleuret[13], M. Fontana[21], F. Fontanelli[25,n], L. F. Foreman[58], R. Forty[44], D. Foulds-Holt[51], M. Franco Sevilla[62], M. Frank[44], E. Franzoso[22,l], G. Frau[18], C. Frei[44], D. A. Friday[58], L. Frontini[26,o], J. Fu[6], Q. Fuehring[16], Y. Fujii[65], T. Fulghesu[14], E. Gabriel[33],

G. Galati[20,i], M. D. Galati[33], A. Gallas Torreira[42], D. Galli[21,j], S. Gambetta[54,44], M. Gandelman[2], P. Gandini[26], H. Gao[6], R. Gao[59], Y. Gao[7], Y. Gao[5], Y. Gao[7], M. Garau[28,k], L. M. Garcia Martin[45], P. Garcia Moreno[41], J. García Pardiñas[44], B. Garcia Plana[42], F. A. Garcia Rosales[13], L. Garrido[41], C. Gaspar[44], R. E. Geertsema[33], L. L. Gerken[16], E. Gersabeck[58], M. Gersabeck[58], T. Gershon[52], Z. Ghorbanimoghaddam[50], L. Giambastiani[29], F. I. Giasemis[14,f], V. Gibson[51], H. K. Giemza[37], A. L. Gilman[59], M. Giovannetti[24], A. Gioventù[42], P. Gironella Gironell[41], C. Giugliano[22,l], M. A. Giza[36], K. Gizdov[54], E. L. Gkougkousis[44], F. C. Glaser[12,18], V. V. Gligorov[14], C. Göbel[66], E. Golobardes[40], D. Golubkov[39], A. Golutvin[57,39,44], A. Gomes[1,2,c,a,*], S. Gomez Fernandez[41], F. Goncalves Abrantes[59], M. Goncerz[36], G. Gong[3], J. A. Gooding[16], I. V. Gorelov[39], C. Gotti[27], J. P. Grabowski[72], L. A. Granado Cardoso[44], E. Graugés[41], E. Graverini[45], L. Grazette[52], G. Graziani, A. T. Grecu[38], L. M. Greeven[33], N. A. Grieser[61], L. Grillo[55], S. Gromov[39], C. Gu[13], M. Guarise[22], M. Guittiere[12], V. Guliaeva[39], P. A. Günther[18], A.-K. Guseinov[39], E. Gushchin[39], Y. Guz[5,39,44], T. Gys[44], T. Hadavizadeh[65], C. Hadjivasiliou[62], G. Haefeli[45], C. Haen[44], J. Haimberger[44], S. C. Haines[51], M. Hajheidari[44], T. Halewood-leagas[56], M. M. Halvorsen[44], P. M. Hamilton[62], J. Hammerich[56], Q. Han[7], X. Han[18], S. Hansmann-Menzemer[18], L. Hao[6], N. Harnew[59], T. Harrison[56], M. Hartmann[12], C. Hasse[44], M. Hatch[44], J. He[6,e], K. Heijhoff[33], F. Hemmer[44], C. Henderson[61], R. D. L. Henderson[65,52], A. M. Hennequin[44], K. Hennessy[56], L. Henry[45], J. Herd[57], J. Heuel[15], A. Hicheur[2], D. Hill[45], M. Hilton[58], S. E. Hollitt[16], J. Horswill[58], R. Hou[7], Y. Hou[9], N. Howarth[56], J. Hu[18], J. Hu[68], W. Hu[5], X. Hu[3], W. Huang[6], X. Huang[70], W. Hulsbergen[33], R. J. Hunter[52], M. Hushchyn[39], D. Hutchcroft[56], P. Ibis[16], M. Idzik[35], D. Ilin[39], P. Ilten[61], A. Inglessi[39], A. Iniukhin[39], A. Ishteev[39], K. Ivshin[39], R. Jacobsson[44], H. Jage[15], S. J. Jaimes Elles[43,71], S. Jakobsen[44], E. Jans[33], B. K. Jashal[43], A. Jawahery[62], V. Jevtic[16], E. Jiang[62], X. Jiang[4,6], Y. Jiang[6], Y. J. Jiang[5], M. John[59], D. Johnson[49], C. R. Jones[51], T. P. Jones[52], S. Joshi[37], B. Jost[44], N. Jurik[44], I. Juszczak[36], D. Kaminaris[45], S. Kandybei[47], Y. Kang[3], M. Karacson[44], D. Karpenkov[39], M. Karpov[39], A. M. Kauniskangas[45], J. W. Kautz[61], F. Keizer[44], D. M. Keller[64], M. Kenzie[51], T. Ketel[33], B. Khanji[64], A. Kharisova[39], S. Kholodenko[30], G. Khreich[12], T. Kirn[15], V. S. Kirsebom[45], O. Kitouni[60], S. Klaver[34], N. Kleijne[30,s], K. Klimaszewski[37], M. R. Kmiec[37], S. Koliiev[48], L. Kolk[16], A. Konoplyannikov[39], P. Kopciewicz[35,44], R. Kopecna[18], P. Koppenburg[33], M. Korolev[39], I. Kostiuk[33], O. Kot[48], S. Kotriakhova, A. Kozachuk[39], P. Kravchenko[39], L. Kravchuk[39], M. Kreps[52], S. Kretzschmar[15], P. Krokovny[39], W. Krupa[64], W. Krzemien[37], J. Kubat[18], S. Kubis[77], W. Kucewicz[36], M. Kucharczyk[36], V. Kudryavtsev[39], E. Kulikova[39], A. Kupsc[78], B. K. Kutsenko[11], D. Lacarrere[44], G. Lafferty[58], A. Lai[28], A. Lampis[28,k], D. Lancierini[46], C. Landesa Gomez[42], J. J. Lane[65], R. Lane[50], C. Langenbruch[18], J. Langer[16], O. Lantwin[39], T. Latham[52], F. Lazzari[30,t], C. Lazzeroni[49], R. Le Gac[11], S. H. Lee[79], R. Lefèvre[10], A. Leflat[39], S. Legotin[39], O. Leroy[11], T. Lesiak[36], B. Leverington[18], A. Li[3], H. Li[68], K. Li[7], L. Li[58], P. Li[44], P.-R. Li[69], S. Li[7], T. Li[4], T. Li[68], Y. Li[7], Y. Li[4], Z. Li[64], Z. Lian[3], X. Liang[64], C. Lin[6], T. Lin[53], R. Lindner[44], V. Lisovskyi[45], R. Litvinov[28,k], G. Liu[68], H. Liu[6], K. Liu[69], Q. Liu[6], S. Liu[4,6], Y. Liu[54], Y. Liu[69], A. Lobo Salvia[41], A. Loi[28], J. Lomba Castro[42], T. Long[51], I. Longstaff[55], J. H. Lopes[2], A. Lopez Huertas[41], S. L.ópez Soliño[42], G. H. Lovell[51], Y. Lu[4,d], C. Lucarelli[23,m], D. Lucchesi[29,q], S. Luchuk[39], M. Lucio Martinez[76], V. Lukashenko[33,48], Y. Luo[3], A. Lupato[29], E. Luppi[22,l], K. Lynch[19], X.-R. Lyu[6], G. M. Ma[3], R. Ma[6], S. Maccolini[16], F. Machefert[12], F. Maciuc[38], I. Mackay[59], L. R. Madhan Mohan[51], M. M. Madurai[49], A. Maevskiy[39], D. Magdalinski[33], D. Maisuzenko[39], M. W. Majewski[35], J. J. Malczewski[36], S. Malde[59], B. Malecki[36,44], L. Malentacca[44], A. Malinin[39], T. Maltsev[39], G. Manca[28,k], G. Mancinelli[11], C. Mancuso[26,12,o], R. Manera Escalero[41], D. Manuzzi[21], D. Marangotto[26,o], J. F. Marchand[9], U. Marconi[21], S. Mariani[44], C. Marin Benito[41,44], J. Marks[18], A. M. Marshall[50], P. J. Marshall[56], G. Martelli[74,r], G. Martellotti[31], L. Martinazzoli[44], M. Martinelli[27,p], D. Martinez Santos[42], F. Martinez Vidal[43], A. Massafferri[1], M. Materok[15], R. Matev[44], A. Mathad[46], V. Matiunin[39], C. Matteuzzi[64,27], K. R. Mattioli[13], A. Mauri[57], E. Maurice[13], J. Mauricio[41], M. Mazurek[44], M. McCann[57], L. Mcconnell[19], T. H. McGrath[58], N. T. McHugh[55], A. McNab[58], R. McNulty[19], B. Meadows[61], G. Meier[16], D. Melnychuk[37], M. Merk[33,76], A. Merli[26,o], L. Meyer Garcia[2], D. Miao[4,6], H. Miao[6], M. Mikhasenko[72,g], D. A. Milanes[71], A. Minotti[27,p], E. Minucci[64], T. Miralles[10], S. E. Mitchell[54], B. Mitreska[16], D. S. Mitzel[16], A. Modak[53], A. Mödden[16], R. A. Mohammed[59], R. D. Moise[15], S. Mokhnenko[39], T. Mombächer[44], M. Monk[52,65], I. A. Monroy[71], S. Monteil[10], A. Morcillo Gomez[42], G. Morello[24], M. J. Morello[30,s], M. P. Morgenthaler[18], J. Moron[35], A. B. Morris[44], A. G. Morris[11], R. Mountain[64], H. Mu[3], Z. M. Mu[5], E. Muhammad[52], F. Muheim[54], M. Mulder[75],

K. Müller[46], F. Muñoz-Rojas[8], R. Murta[57], P. Naik[56], T. Nakada[45], R. Nandakumar[53], T. Nanut[44], I. Nasteva[2], M. Needham[54], N. Neri[26,o], S. Neubert[72], N. Neufeld[44], P. Neustroev[39], R. Newcombe[57], J. Nicolini[16,12], D. Nicotra[76], E. M. Niel[45], N. Nikitin[39], P. Nogga[72], N. S. Nolte[60], C. Normand[9,k,28], J. Novoa Fernandez[42], G. Nowak[61], C. Nunez[79], H. N. Nur[55], A. Oblakowska-Mucha[35], V. Obraztsov[39], T. Oeser[15], S. Okamura[22,l,44], R. Oldeman[28,k], F. Oliva[54], M. Olocco[16], C. J. G. Onderwater[76], R. H. O'Neil[54], J. M. Otalora Goicochea[2], T. Ovsiannikova[39], P. Owen[46], A. Oyanguren[43], O. Ozcelik[54], K. O. Padeken[72], B. Pagare[52], P. R. Pais[18], T. Pajero[59], A. Palano[20], M. Palutan[24], G. Panshin[39], L. Paolucci[52], A. Papanestis[53], M. Pappagallo[20,i], L. L. Pappalardo[22,l], C. Pappenheimer[61], C. Parkes[58,44], B. Passalacqua[22,l], G. Passaleva[23], D. Passaro[30,s], A. Pastore[20], M. Patel[57], J. Patoc[59], C. Patrignani[21,j], C. J. Pawley[76], A. Pellegrino[33], M. Pepe Altarelli[24], S. Perazzini[21], D. Pereima[39], A. Pereiro Castro[42], P. Perret[10], A. Perro[44], K. Petridis[50], A. Petrolini[25,n], S. Petrucci[54], H. Pham[64], L. Pica[30,s], M. Piccini[74], B. Pietrzyk[9], G. Pietrzyk[12], D. Pinci[31], F. Pisani[44], M. Pizzichemi[27,p], V. Placinta[38], M. Plo Casasus[42], F. Polci[14,44], M. Poli Lener[24], A. Poluektov[11], N. Polukhina[39], I. Polyakov[44], E. Polycarpo[2], S. Ponce[44], D. Popov[6], S. Poslavskii[39], K. Prasanth[36], L. Promberger[18], C. Prouve[42], V. Pugatch[48], V. Puill[12], G. Punzi[30,t], H. R. Qi[3], W. Qian[6], N. Qin[3], S. Qu[3], R. Quagliani[45], B. Rachwal[35], J. H. Rademacker[50], M. Rama[30], M. Ramírez García[79], M. Ramos Pernas[52], M. S. Rangel[2], F. Ratnikov[39], G. Raven[34], M. Rebollo De Miguel[43], F. Redi[44], J. Reich[50], F. Reiss[58], Z. Ren[3], P. K. Resmi[59], R. Ribatti[30,s], G. R. Ricart[13,80], D. Riccardi[30,s], S. Ricciardi[53], K. Richardson[60], M. Richardson-Slipper[54], K. Rinnert[56], P. Robbe[12], G. Robertson[54], E. Rodrigues[56,44], E. Rodriguez Fernandez[42], J. A. Rodriguez Lopez[71], E. Rodriguez Rodriguez[42], A. Rogovskiy[53], D. L. Rolf[44], A. Rollings[59], P. Roloff[44], V. Romanovskiy[39], M. Romero Lamas[42], A. Romero Vidal[42], G. Romolini[22], F. Ronchetti[45], M. Rotondo[24], M. S. Rudolph[64], T. Ruf[44], R. A. Ruiz Fernandez[42], J. Ruiz Vidal[43], A. Ryzhikov[39], J. Ryzka[35], J. J. Saborido Silva[42], N. Sagidova[39], N. Sahoo[49], B. Saitta[28,k], M. Salomoni[44], C. Sanchez Gras[33], I. Sanderswood[43], R. Santacesaria[31], C. Santamarina Rios[42], M. Santimaria[24], L. Santoro[1], E. Santovetti[32], D. Saranin[39], G. Sarpis[54], M. Sarpis[72], A. Sarti[31], C. Satriano[31,u], A. Satta[32], M. Saur[5], D. Savrina[39], H. Sazak[10], L. G. Scantlebury Smead[59], A. Scarabotto[14], S. Schael[15], S. Scherl[56], A. M. Schertz[73], M. Schiller[55], H. Schindler[44], M. Schmelling[17], B. Schmidt[44], S. Schmitt[15], O. Schneider[45], A. Schopper[44], N. Schulte[16], S. Schulte[45], M. H. Schune[12], R. Schwemmer[44], G. Schwering[15], B. Sciascia[24], A. Sciuccati[44], S. Sellam[42], A. Semennikov[39], M. Senghi Soares[34], A. Sergi[25,n], N. Serra[46,44], L. Sestini[29], A. Seuthe[16], Y. Shang[5], D. M. Shangase[79], M. Shapkin[39], I. Shchemerov[39], L. Shchutska[45], T. Shears[56], L. Shekhtman[39], Z. Shen[5], S. Sheng[4,6], V. Shevchenko[39], B. Shi[6], E. B. Shields[27,p], Y. Shimizu[12], E. Shmanin[39], R. Shorkin[39], J. D. Shupperd[64], B. G. Siddi[22,l], R. Silva Coutinho[64], G. Simi[29], S. Simone[20,i], M. Singla[65], N. Skidmore[58], R. Skuza[18], T. Skwarnicki[64], M. W. Slater[49], J. C. Smallwood[59], J. G. Smeaton[51], E. Smith[60], K. Smith[63], M. Smith[57], A. Snoch[33], L. Soares Lavra[54], M. D. Sokoloff[61], F. J. P. Soler[55], A. Solomin[39,50], A. Solovev[39], I. Solovyev[39], R. Song[65], Y. Song[45], Y. Song[3], Y. S. Song[5], F. L. Souza De Almeida[2], B. Souza De Paula[2], E. Spadaro Norella[26,o], E. Spedicato[21], J. G. Speer[16], E. Spiridenkov[39], P. Spradlin[55], V. Sriskaran[44], F. Stagni[44], M. Stahl[44], S. Stahl[44], S. Stanislaus[59], E. N. Stein[44], O. Steinkamp[46], O. Stenyakin[39], H. Stevens[16], D. Strekalina[39], Y. Su[6], F. Suljik[59], J. Sun[28], L. Sun[70], Y. Sun[62], P. N. Swallow[49], K. Swientek[35], F. Swystun[52], A. Szabelski[37], T. Szumlak[35], M. Szymanski[44], Y. Tan[3], S. Taneja[58], M. D. Tat[59], A. Terentev[46], F. Terzuoli[30,w], F. Teubert[44], E. Thomas[44], D. J. D. Thompson[49], H. Tilquin[57], V. Tisserand[10], S. T'Jampens[9], M. Tobin[4], L. Tomassetti[22,l], G. Tonani[26,o], X. Tong[5], D. Torres Machado[1], L. Toscano[16], D. Y. Tou[3], C. Trippl[45], G. Tuci[18], N. Tuning[33], L. H. Uecker[18], A. Ukleja[37], D. J. Unverzagt[18], E. Ursov[39], A. Usachov[34], A. Ustyuzhanin[39], U. Uwer[18], V. Vagnoni[21], A. Valassi[44], G. Valenti[21], N. Valls Canudas[40], M. Van Dijk[45], H. Van Hecke[63], E. van Herwijnen[57], C. B. Van Hulse[42,y], R. Van Laak[45], M. van Veghel[33], R. Vazquez Gomez[41], P. Vazquez Regueiro[42], C. V.ázquez Sierra[42], S. Vecchi[22], J. J. Velthuis[50], M. Veltri[23,x], A. Venkateswaran[45], M. Vesterinen[52], D. Vieira[61], M. Vieites Diaz[44], X. Vilasis-Cardona[40], E. Vilella Figueras[56], A. Villa[21], P. Vincent[14], F. C. Volle[12], D. vom Bruch[11], V. Vorobyev[39], N. Voropaev[39], K. Vos[76], C. Vrahas[54], J. Walsh[30], E. J. Walton[65], G. Wan[5], C. Wang[18], G. Wang[7], J. Wang[5], J. Wang[4], J. Wang[3], J. Wang[70], M. Wang[26], N. W. Wang[6], R. Wang[50], X. Wang[68], Y. Wang[7], Z. Wang[46], Z. Wang[3], Z. Wang[6], J. A. Ward[52,65], N. K. Watson[49], D. Websdale[57], Y. Wei[5], B. D. C. Westhenry[50], D. J. White[58], M. Whitehead[55], A. R. Wiederhold[52], D. Wiedner[16], G. Wilkinson[59], M. K. Wilkinson[61], I. Williams[51], M. Williams[60], M. R. J. Williams[54], R. Williams[51], F. F. Wilson[53], W. Wislicki[37], M. Witek[36], L. Witola[18], C. P. Wong[63],

G. Wormser[12], S. A. Wotton[51], H. Wu[64], J. Wu[7], Y. Wu[5], K. Wyllie[44], S. Xian[68], Z. Xiang[4], Y. Xie[7], A. Xu[30], J. Xu[6], L. Xu[3], L. Xu[3], M. Xu[52], Z. Xu[10], Z. Xu[6], Z. Xu[4], D. Yang[3], S. Yang[6], X. Yang[5], Y. Yang[25,n], Z. Yang[5], Z. Yang[62], V. Yeroshenko[12], H. Yeung[58], H. Yin[7], C. Y. Yu[5], J. Yu[67], X. Yuan[4], E. Zaffaroni[45], M. Zavertyaev[17], M. Zdybal[36], M. Zeng[3], C. Zhang[5], D. Zhang[7], J. Zhang[6], L. Zhang[3], S. Zhang[67], S. Zhang[5], Y. Zhang[5], Y. Zhang[59], Y. Z. Zhang[3], Y. Zhao[18], A. Zharkova[39], A. Zhelezov[18], X. Z. Zheng[3], Y. Zheng[6], T. Zhou[5], X. Zhou[7], Y. Zhou[6], V. Zhovkovska[12], L. Z. Zhu[6], X. Zhu[3], X. Zhu[7], Z. Zhu[6], V. Zhukov[15,39], J. Zhuo[43], Q. Zou[4,6], S. Zucchelli[21,j], D. Zuliani[29], G. Zunica[58]

1 Centro Brasileiro de Pesquisas Físicas (CBPF), Rio de Janeiro, Brazil
2 Universidade Federal do Rio de Janeiro (UFRJ), Rio de Janeiro, Brazil
3 Center for High Energy Physics, Tsinghua University, Beijing, China
4 Institute Of High Energy Physics (IHEP), Beijing, China
5 School of Physics State Key Laboratory of Nuclear Physics and Technology, Peking University, Beijing, China
6 University of Chinese Academy of Sciences, Beijing, China
7 Institute of Particle Physics, Central China Normal University, Wuhan, Hubei, China
8 Consejo Nacional de Rectores (CONARE), San Jose, Costa Rica
9 Université Savoie Mont Blanc, CNRS, IN2P3-LAPP, Annecy, France
10 Université Clermont Auvergne, CNRS/IN2P3, LPC, Clermont-Ferrand, France
11 Aix Marseille Univ, CNRS/IN2P3, CPPM, Marseille, France
12 Université Paris-Saclay, CNRS/IN2P3, IJCLab, Orsay, France
13 Laboratoire Leprince-Ringuet, CNRS/IN2P3, Ecole Polytechnique, Institut Polytechnique de Paris, Palaiseau, France
14 LPNHE, Sorbonne Université, Paris Diderot Paris Cité, CNRS/IN2P3, Paris, France
15 I. Physikalisches Institut, RWTH Aachen University, Aachen, Germany
16 Fakultät Physik, Technische Universität Dortmund, Dortmund, Germany
17 Max-Planck-Institut für Kernphysik (MPIK), Heidelberg, Germany
18 Physikalisches Institut, Ruprecht-Karls-Universität Heidelberg, Heidelberg, Germany
19 School of Physics, University College Dublin, Dublin, Ireland
20 INFN Sezione di Bari, Bari, Italy
21 INFN Sezione di Bologna, Bologna, Italy
22 INFN Sezione di Ferrara, Ferrara, Italy
23 INFN Sezione di Firenze, Firenze, Italy
24 INFN Laboratori Nazionali di Frascati, Frascati, Italy
25 INFN Sezione di Genova, Genova, Italy
26 INFN Sezione di Milano, Milano, Italy
27 INFN Sezione di Milano-Bicocca, Milano, Italy
28 INFN Sezione di Cagliari, Monserrato, Italy
29 Università degli Studi di Padova, Università e INFN, Padova, Padova, Italy
30 INFN Sezione di Pisa, Pisa, Italy
31 INFN Sezione di Roma La Sapienza, Roma, Italy
32 INFN Sezione di Roma Tor Vergata, Roma, Italy
33 Nikhef National Institute for Subatomic Physics, Amsterdam, The Netherlands
34 Nikhef National Institute for Subatomic Physics and VU University Amsterdam, Amsterdam, The Netherlands
35 AGH - University of Science and Technology, Faculty of Physics and Applied Computer Science, Kraków, Poland
36 Henryk Niewodniczanski Institute of Nuclear Physics Polish Academy of Sciences, Kraków, Poland
37 National Center for Nuclear Research (NCBJ), Warsaw, Poland
38 Horia Hulubei National Institute of Physics and Nuclear Engineering, Bucharest-Magurele, Romania
39 Affiliated with an institute covered by a cooperation agreement with CERN, Geneva, Switzerland
40 DS4DS, La Salle, Universitat Ramon Llull, Barcelona, Spain
41 ICCUB, Universitat de Barcelona, Barcelona, Spain
42 Instituto Galego de Física de Altas Enerxías (IGFAE), Universidade de Santiago de Compostela, Santiago de Compostela, Spain
43 Instituto de Fisica Corpuscular, Centro Mixto Universidad de Valencia - CSIC, Valencia, Spain
44 European Organization for Nuclear Research (CERN), Geneva, Switzerland

[45] Institute of Physics, Ecole Polytechnique Fédérale de Lausanne (EPFL), Lausanne, Switzerland

[46] Physik-Institut, Universität Zürich, Zürich, Switzerland

[47] NSC Kharkiv Institute of Physics and Technology (NSC KIPT), Kharkiv, Ukraine

[48] Institute for Nuclear Research of the National Academy of Sciences (KINR), Kyiv, Ukraine

[49] University of Birmingham, Birmingham, UK

[50] H.H. Wills Physics Laboratory, University of Bristol, Bristol, UK

[51] Cavendish Laboratory, University of Cambridge, Cambridge, UK

[52] Department of Physics, University of Warwick, Coventry, UK

[53] STFC Rutherford Appleton Laboratory, Didcot, UK

[54] School of Physics and Astronomy, University of Edinburgh, Edinburgh, UK

[55] School of Physics and Astronomy, University of Glasgow, Glasgow, UK

[56] Oliver Lodge Laboratory, University of Liverpool, Liverpool, UK

[57] Imperial College London, London, UK

[58] Department of Physics and Astronomy, University of Manchester, Manchester, UK

[59] Department of Physics, University of Oxford, Oxford, UK

[60] Massachusetts Institute of Technology, Cambridge, MA, USA

[61] University of Cincinnati, Cincinnati, OH, USA

[62] University of Maryland, College Park, MD, USA

[63] Los Alamos National Laboratory (LANL), Los Alamos, NM, USA

[64] Syracuse University, Syracuse, NY, USA

[65] School of Physics and Astronomy, Monash University, Melbourne, Australia associated to[52]

[66] Pontifícia Universidade Católica do Rio de Janeiro (PUC-Rio), Rio de Janeiro, Brazil associated to[2]

[67] School of Physics and Electronics, Hunan University, Changsha City, China associated to[7]

[68] Guangdong Provincial Key Laboratory of Nuclear Science, Guangdong-Hong Kong Joint Laboratory of Quantum Matter, Institute of Quantum Matter, South China Normal University, Guangzhou, China associated to[3]

[69] Lanzhou University, Lanzhou, China associated to[4]

[70] School of Physics and Technology, Wuhan University, Wuhan, China associated to[3]

[71] Departamento de Fisica, Universidad Nacional de Colombia, Bogota, Colombia associated to[14]

[72] Universität Bonn - Helmholtz-Institut für Strahlen und Kernphysik, Bonn, Germany associated to[18]

[73] Eotvos Lorand University, Budapest, Hungary associated to[44]

[74] INFN Sezione di Perugia, Perugia, Italy associated to[22]

[75] Van Swinderen Institute, University of Groningen, Groningen, The Netherlands associated to[33]

[76] Universiteit Maastricht, Maastricht, The Netherlands associated to[33]

[77] Tadeusz Kosciuszko Cracow University of Technology, Cracow, Poland associated to[36]

[78] Department of Physics and Astronomy, Uppsala University, Uppsala, Sweden associated to[55]

[79] University of Michigan, Ann Arbor, Ann Arbor, MI, USAassociated to[64]

[80] Departement de Physique Nucleaire (SPhN), Gif-Sur-Yvette, France

[a] Universidade de Brasília, Brasília, Brazil

[b] Centro Federal de Educacão Tecnológica Celso Suckow da Fonseca, Rio De Janeiro, Brazil

[c] Universidade Federal do Triângulo Mineiro (UFTM), Uberaba-MG, Brazil

[d] Central South U, Changsha, China

[e] Hangzhou Institute for Advanced Study, UCAS, Hangzhou, China

[f] LIP6, Sorbonne Universite, Paris, France

[g] Excellence Cluster ORIGINS, Munich, Germany

[h] Universidad Nacional Autónoma de Honduras, Tegucigalpa, Honduras

[i] Università di Bari, Bari, Italy

[j] Università di Bologna, Bologna, Italy

[k] Università di Cagliari, Cagliari, Italy

[l] Università di Ferrara, Ferrara, Italy

[m] Università di Firenze, Firenze, Italy

[n] Università di Genova, Genova, Italy

[o] Università degli Studi di Milano, Milano, Italy

[p] Università di Milano Bicocca, Milano, Italy

[q] Università di Padova, Padova, Italy

[r] Università di Perugia, Perugia, Italy

[s] Scuola Normale Superiore, Pisa, Italy

[t] Università di Pisa, Pisa, Italy

[u] Università della Basilicata, Potenza, Italy

[v] Università di Roma Tor Vergata, Roma, Italy

[w] Università di Siena, Siena, Italy

[x] Università di Urbino, Urbino, Italy

[y] Universidad de Alcalá, Alcalá de Henares, Spain

[z] Universidade da Coruña, Coruña, Spain

*Deceased